ARTICLE

Pixelated frequency-agile metasurface for broadband terahertz molecular fingerprint sensing

Received 00th January 20xx,
Accepted 00th January 20xx

DOI: 10.1039/x0xx00000x

Lang Sun,[a] Ride Wang,[a] Lei Xu,[b] Jiayi Wang,[c] Yanan Jiao,[d] Zenghong Ma,[e] Zhaofu Ma,[d] Chao Chang,*[,a,f] and Xiao Yang,*[,a]

Terahertz (THz) plasmonic resonance based on the arbitrarily designed resonance metasurface is the key technique of choice for enhancing fingerprint absorption spectroscopy identification of biomolecules. Here, we report a broadband THz micro-photonics sensor based on the pixelated frequency-agile metasurface and illustrate its application ability to enhance and differentiate the detection of broadband absorption fingerprint spectrum. The design uses symmetrical metal C-shaped resonators with the functional graphene micro-ribbons selectively patterned into the gaps. The excited toroidal dipole (TD) of individual frequency-agile meta-unit was demonstrated by the head-to-tail arrangement of the magnetic dipoles, whose resonance positions are near linearly modulated with the varying Femi lever of graphene. The configuration arranges a certain metapixel of the metasurface to multiple response spectra assembling a one-to-many mapping between spatial and spectral information which is instrumental in greatly shrinking the actual size of the sensor. By the synchronous regulation of graphene and C-shape rings, we have obtained highly surface-sensitive resonances over a wide spectral range (~ 1.5 THz) with a spectral resolution less than 20 GHz. The target multiple enhanced absorption spectrum of glucose molecules is read out in a broadband region with high sensitivity. More importantly, the design can be extended to cover a larger spectral region by altering the range of geometrical parameters. Our microphotonic technique can resolve absorption fingerprints without the need for spectrometry and frequency scanning, thereby providing an approach for highly sensitive and versatile miniaturized THz spectroscopy devices.

1 Introduction

The terahertz (THz) spectroscopy is of the essence for label-free and non-destructive sensing since it covers the characteristic biomolecular absorption fingerprints rooted in the intrinsic molecular rotational and vibrational modes.[1,2] However, THz wavelength mismatches with the absorption cross-section of the analyte, which leads to relatively weak light-matter interactions at the micrometric size. It significantly impedes the widespread application of THz technology in practical biochemical molecular recognition. The proposed micro/nano-photonics can overcome the bottleneck by strongly enhancing the near-field of subwavelength resonators to address some THz practical applications,[3-12]which promote unprecedented control of light at will. If the resonance and absorption fingerprints luckily overlap in the spectrum, the enhanced near-field will intensify the molecular-resonator coupling,[13-16] which greatly affects the linewidth and intensity of the resonance, so that the molecular fingerprints can be extracted from the change. Nevertheless, the achieved performance is still far from ideal since the resonant of the unit is easily affected by the surrounding environment and exhibits frequency drift, which leads to the misalignment of the designed overlap. Meanwhile, the inspection of a single characteristic fingerprint of analyte easily causes a "false positive" diagnosis. In order to accurately detect the multi-fingerprints spectrum of the analyte, the broadband waveguide modes supported by microrod array metasurface or spoof surface plasmon are studied to achieve this goal. The existing cut-off frequency of the waveguide mode limits the practical application of wider-spectrum sensing enhancement.[17,18] Further, Hatice Altug et al. illustrated imaging-based molecular barcoding with pixelated dielectric metasurfaces, which cover a larger spectrum region.[19] However, miniaturizing device footprints as a major challenge still exist at the device level that prevents reliable, large-scale THz system integration. The proposed functional tunable metamaterial can achieve continuous adjustment on the resonance frequency, and exhibits great potential in the development of driving the miniaturization of the device.

[a.] *Innovation Laboratory of Terahertz Biophysics, National Innovation Institute of Defense Technology, Beijing, 100071, China. E-mail: gwyzlzssb@pku.edu.cn*
[b.] *Advanced Optics and Photonics Laboratory, Department of Engineering, School of Science and Technology, Nottingham Trent University, Nottingham NG11 8NS, UK.*
[c.] *Key Laboratory of Weak-Light Nonlinear Photonics, Ministry of Education, TEDA Institute of Applied Physics and School of Physics, Nankai University, Tianjin 300457, China.*
[d.] *Department of General Surgery, First Medical Center of Chinese PLA General Hospital, Beijing 100853, People's Republic of China.*
[e.] *The Science and Technology Development Fund of Tianjin Education Commission for Higher Education*
[f.] *School of Physics, Peking University, Beijing, 100871, China.*

Here, we developed an ultra-broadband THz metasensor that introduced the basic concept of the pixel through a combination of symmetrical metal C-shape plasmonic resonators and tunable graphene micro-ribbons to detect fingerprint spectra. The resonance positions of individual frequency-agile metapixels are linearly modulated with the varying of Femi energy over a target THz fingerprint range. This configuration allows a specific metapixel of the metasurface to be assigned to multiple characteristic fingerprints, establishing a one-to-many mapping between spatial and spectral signals. The near-unity response of the designed resonant structure is fairly clean without additional loss, and its unique properties allow us to accurately enhance the detection of rich molecular fingerprint spectra. By comparing the readouts of the absorption spectra with and without metasurface, the method of our research is demonstrated to suit advanced broadband chemical identification and component analysis.

2 Design and simulation method

Fig. 1(a) illustrates the schematic diagram of the pixelated-based frequency-agile metasensor, which contains symmetrical C-shape rings of different radiuses combining with graphene micro-ribbon arrays on the quartz substrate. Such structure can enhance the detection of broadband absorption fingerprint spectrum and improve the spectral resolution (~ GHz). The inset shows the geometry parameters of the unit cell. The graphene micro-ribbon is a single layer. To figure out the characteristics of the designed metamaterials, we simulate the light characteristics from the design based on 3D finite-difference time-domain (FDTD) solutions software. In the simulation, the perfectly matched layer (PML) at *z* direction and the periodic boundary condition at the *x* and *y* directions were applied. The material of symmetric rings is set to the perfect electrical conductor (PEC) since the conductivity is at the order of 10^7 S/m in the THz band. Fig. 1(b) gives the reflection spectrum of the resonator with r = 11 μm without graphene when the incident light is polarized along the *y* axis. To reveal the resonance mechanism of the proposed structure, we further calculate the distribution of electric field amplitude and the current density at its resonance frequency as depicted in Fig. 1(c) and Fig. 1(d), respectively. As can be seen, a significant enhancement of the electric field (59-fold) is observed at the resonance frequency f = 1.4 THz. The electric and magnetic field configurations are analyzed which indicate a strong toroidal dipole (TD) mode excitation.[20-22] TD can enhance energy localization through concentrating time-varying magnetic field in a small circular area, i.e., the toroidal current and poloidal magnetic field distributions around the mirror symmetry C-shape rings. This head-to-tail alignment of magnetic dipole leads to coupling between the nearby C-shape rings in the unit cell via circulating magnetic fields, and forming toroidal moment. Due to the toroidal moment, the coupling between mirror symmetrical C-shape rings is enhanced, and the radiation loss between the resonators and the free space is suppressed, which is responsible for the enhanced quality factor response.

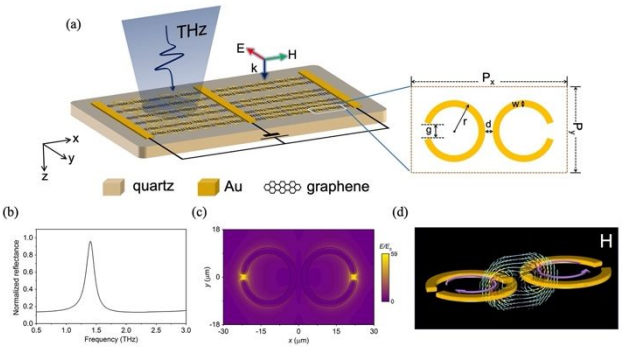

Fig. 1 (a) Schematic diagram of enhanced absorption fingerprint spectra detection based on THz pixelated frequency-agile metasurface. The inset depicts the geometrical parameters of the unit cell, which consists of symmetrical C-shape rings. The graphene micro-ribbons are embedded in the gap. The fixed opening size of the split g = 2 μm, the linewidth w = 2 μm, the interval between the rings d = 2 μm and the variable r is the radius of the ring. The periods in the *x* and *y* directions are P_x and P_y, respectively. (b) The calculated reflectance spectrum of the symmetrical C-shape rings with a fixed radius r = 11 μm. (c) Electric field intensity is confined in the capacitive gaps with an enhancement of up to 59. (d) A clear in-plane TD excitation due to the anti-phase magnetic field. The pink arrows indicate the excited surface current of the rings.

The schematic illustration of the working principle of our metasensor is shown in Fig. 2(a). The giant tunable span of the resonance is achieved by varying the Femi level of the graphene micro-ribbon embedded in the gaps since it is placed in the near-field. The electromagnetic properties of graphene have a large impact on the electric field response of the rings, and strongly affect the resonance of the meta-atoms, thereby achieving more precise tunability.[12] The surface conductivity σ of infinitely thin graphene monolayer related to Fermi level, consisting of intraband σ_{intra} and interband σ_{inter} transition, can be expressed as: [23-27]

$$\sigma = \sigma_{inter} + \sigma_{intra}$$

The contribution of interband transition compared with the intraband transition can be negligible in the THz region. The intraband conductivity can be expressed as an expression like the Drude-like model:

$$\sigma_{intra} = \frac{ie^2 E_f}{\pi \hbar^2 (w + i\tau^{-1})}$$

where $\hbar$ and E_f are the Planck constant and the Fermi level of graphene, respectively. The $\tau = \mu E_f / ev_f^2$ is the carrier relaxation time. The Fermi velocity is $v_f = 10^6$ m/s, and μ is the carrier mobility.[28,29] The normalized reflectance spectra of meta-atom is shown in Fig. 2(b). It can be seen that a regular blueshift of the resonance frequency between 1.82 and 2.27 THz as E_f increases from 0 to 0.3 eV in a fixed step of 0.02 eV. In order to quantitatively analyze the influence of the Fermi level on the resonance frequency, we introduce frequency variation Δf, which is defined as $\Delta f = (f - f_0) / f_0$, where f represents the

resonance frequency of graphene at different E_f values, and f_0 represents the resonance frequency in metamaterials without graphene. Fig. 2(c) shows the frequency variation with the increase of graphene E_f value. The results demonstrate an approximately linear relationship between the frequency shift and applied E_f, indicating a frequency shift rate of 120 GHz per 0.1 eV, which indicates that the proposed frequency-agile structure acts as an effective device working on a wide range of frequencies. Based on this relationship, through voltage bias or chemical doping, graphene can provide powerful ultra-wideband tuning.

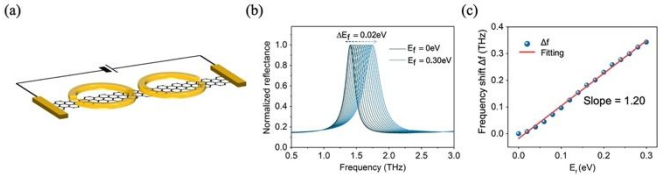

Fig. 2 (a) Sketch view of the frequency-agile meta-atom. The typical graphene micro-ribbon is placed in the centre whose carrier concentration is controlled by Femi energy. (b) Normalized reflectance spectra of the unit cell of individual metapixel exhibit the blue shifts as a function of different Fermi energies from E_f = 0 eV to E_f = 0.3 eV with a fixed dimension of the radius r = 11 μm. (c) The corresponding tips of the resonance shift as a function of gradual E_f values.

3 Results and Discussion

We then use the unit arrays of the different radiuses with the graphene micro-ribbons to constitute the pixelated metasurface as shown in Fig. 3(a). This design assigns each metapixel area to a certain responsive region, forming a one-to-many mapping between spatial and spectral information. The characteristic radiuses of the symmetrical C-shape rings are shown in Fig. 3(b). It is well-known that graphene has a strong ability to adjust the resonance frequency of the structure. We numerically simulated the normalized reflectance spectra of 6 exemplary pixel areas with a varying radius of the rings, and obtained near-unity reflectance intensity and linear adjustability of the resonance positions covering the spectral range from 1.2 to 2.7 THz as shown in Fig. 3(c). This corresponds to a spectral resolution of 20 GHz. The resolution capability of the device depends on the minimum step-length for the Fermi level. Note that our design can easily be extended to cover a larger spectral region by varying the range of geometrical scaling parameters and the E_f of the graphene.

We illustrate molecular fingerprint detection by covering the glucose on the metasurface as shown in Fig. 4(a). The Lorentz dispersion model is chosen as the dielectric function of glucose to demonstrate its characteristic absorption spectra, whose corresponding frequencies in detail are 1.229, 1.446, 1.530, 1.610, 1.811, and 1.996 THz, respectively.[30] We assess the capability of our metasensor for fingerprint detection by

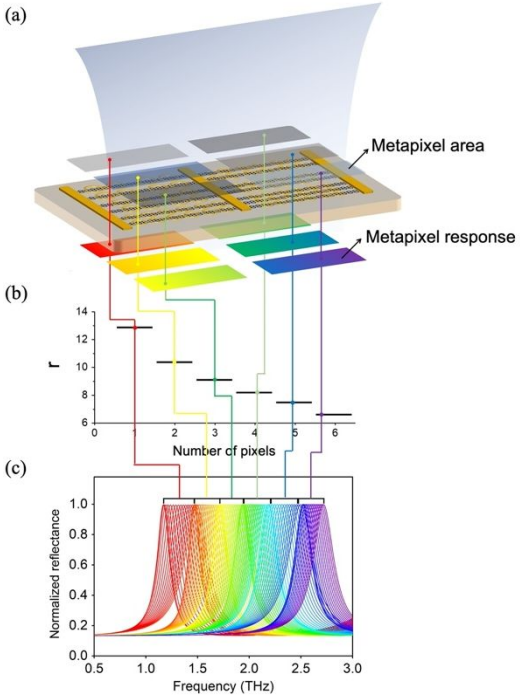

Fig. 3 (a) Pixelated metasurface composed of a two-dimensional array of symmetric rings and graphene micro-ribbons. The resonance frequencies are tuned over a continuous spectral range. Different pixelated areas (gray rectangles) cover corresponding spectral ranges (rectangles for color gradient). (b) The scaling dimensions of the metasurface elements that make up the sensor. Designed geometrical parameters are r = 12.9 μm, 10.4 μm, 9.1 μm, 8.2 μm, 7.5 μm, and 6.6 μm, respectively. (c) Numerically simulated metapixel reflectance spectra for different values of the scaling parameter r with gradient corresponding Femi level are arranged to cover the continuous spectrum.

calculating the reflectance and transmission intensity from the spectral data of each metapixel. These signals are analogous to a readout of the metasurface optical response without and with the glucose layer in Fig. 4(b). The normalized reflectance spectra before and after glucose physisorption are shown in the top and middle panels of Fig. 4(c), respectively. All spectra are normalized to the peak reflectance values of reference measurements without glucose. It can be seen that the normalized spectra after glucose physisorption have an obvious attenuation, which is caused by the absorption characteristics of the glucose. In order to quantify this attenuation change, the absorbance signal is defined as $A = -\log_{10}(R_g/R_0)$, where R_0 and R_g are the envelope of peak reflectance before and after glucose absorption, respectively. The absorption characteristics of glucose molecules are revealed by calculating the absorbance signal A, as shown in the bottom panel in Fig. 4(c), which is in good agreement with the material absorbance characteristic signal (solid line) without metasurface. The absorptance is

improved as much as nearly 5 times. By comparing the information readout with or without target analyte molecules, we proved that the platform has great potential in biochemical analysis and component identification.

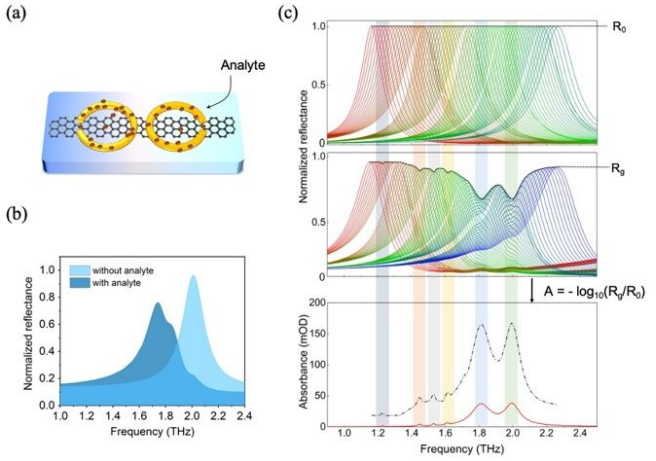

Fig. 4 (a) Rendered sketch showing controlled biomolecule delivery to the sensor surface for microarray-based detection. (b) The effect of analytes on the reflection spectrum when the E_f = 0.12 eV and R = 8.2 μm. (c) Fingerprint retrieval and spatial absorption mapping of the glucose. The top panel is the normalized reflectance spectra before glucose physisorption. The middle panel is the normalized reflectance spectra after glucose physisorption. The variation radiuses of the metal units constituting the metasurface are r = 12.5 μm, 10.4 μm, 9.1 μm, 8.2 μm, and 7.5 μm, respectively. The bottom panel is the glucose absorption fingerprint calculated from the reflectance spectrum envelope before and after glucose physisorption with (the dashed line) and without (the solid line) metasurface.

4 Conclusions

In summary, we have demonstrated a high-resolution THz molecular fingerprint metasensor that can significantly expand the working bandwidth based on the pixelated frequency-agile metasurface. An unprecedented design of incorporation between symmetrical metal C-shaped resonators and tunable graphene micro-ribbons selectively placed into the gaps was applied to cover the target THz fingerprint range. The excited TD mode was demonstrated by the head-to-tail circulating magnetic field arrangement. The design can arrange a certain metapixel of the metasurface to multiple characteristic absorption spectra establishing a one-to-many mapping between spatial and spectral information, which have a footprint much smaller than conventional metasensor. In addition, a stronger confined near-field enhancement and more powerful adjustability can be achieved through a more complex arrangement of meta-atoms and functional materials. The broadband THz fingerprint spectrum obtained based on our method would open new avenues for versatile and broadband miniaturized THz functional elements.

Conflicts of interest

The authors declare no conflict of interest.

Acknowledgements

This work was supported by the XPLORER PRIZE; Research Project of Tianjin Municipal Education Commission (2020KJ088).

Notes and references

1 A. Ahmadivand, B. Gerislioglu, R. Ahuja and Y. K. Mishra, *Mater. Today*, 2020, **32**, 108-130.
2 Y. Xiang, Z. Xiang, Y. Ke, Y. Liu and L. Yang, *Trends Biotechnol.*, 2016, **34**, 810-824.
3 N. F. Yu and F. Capasso, *Nat. Mater.*, 2014, **13**, 139-150.
4 M. J. Lagos, A. Trugler, U. Hohenester and P. E. Batson, *Nature*, 2017, **543**, 529-532.
5 C. R. Williams, S. R. Andrews, S. A. Maier, A. I. Fernandez-Dominguez, L. Martin-Moreno and F. J. Garcia-Vidal, *Nat. Photonics*, 2008, **2**, 175-179.
6 R. Wang, L. Xu, J. Y. Wang, L. Sun, Y. N. Jiao, Y. Meng, S. Chen, C. Chang and C. H. Fan, *Nanoscale*, 2021, **13**, 18467-18472.
7 M. L. Tseng, A. Jahani, A. Leitis and H. Altug, *Acs Photonics*, 2021, **8**, 47-60.
8 C. Mathai, R. Jain, V. G. Achanta, S. P. Duttagupta, D. Ghindani, N. R. Josh, R. Pinto and S. S. Prabhu, *Opt. Lett.*, 2018, **43**, 5383-5386.
9 X. F. Zang, W. W. Xu, M. Gu, B. S. Yao, L. Chen, Y. Peng, J. Y. Xie, A. V. Balakin, A. P. Shkurinov, Y. M. Zhu and S. L. Zhuang, *Adv. Opt. Mater.*, 2019, **8**.
10 R. D. Wang, Q. Wu, W. Cai, Q. Zhang, H. Xiong, B. Zhang, J. W. Qi, J. H. Yao and J. J. Xu, *Acs Photonics*, 2019, **6**, 1774-1779.
11 J. Y. Wang, Y. Liu, D. H. Yang, Z. C. Hu, X. Z. Zhang, S. Q. Xia, D. H. Song, M. X. Ren, S. H. Gao, R. D. Wang, Z. G. Chen and J. J. Xu, *Opt. Express*, 2021, **29**, 19531-19539.
12 X. Y. Liu, Z. Z. Liu, M. Hua, L. Y. Wang, K. F. Wang, W. W. Zhang, Y. F. Ning, Y. P. Shi, X. D. Wang and F. H. Yang, *Acs Appl. Nano Mater.*, 2020, **3**, 2129-2133.
13 W. W. Tang, L. Wang, X. S. Chen, C. L. Liu, A. Q. Yu and W. Lu, *Nanoscale*, 2016, **8**, 15196-15204.
14 J. X. Wei, Y. Li, Y. H. Chang, D. M. N. Hasan, B. W. Dong, Y. M. Ma, C. W. Qiu and C. Lee, *Acs Appl. Mater. Interfaces*, 2019, **11**, 47270-47278.
15 D. Rodrigo, A. Tittl, N. Ait-Bouziad, A. John-Herpin, O. Limaj, C. Kelly, D. Yoo, N. J. Wittenberg, S. H. Oh, H. A. Lashuel and H. Altug, *Nat. Commun.*, 2018, **9**, 1-9.
16 B. J. Han, Z. H. Han, J. Y. Qin, Y. M. Wang and Z. S. Zhao, *Talanta*, 2019, **192**, 1-5.
17 B. H. Ng, S. M. Hanham, J. F. Wu, A. I. Fernandez-Dominguez, N. Klein, Y. F. Liew, M. B. H. Breese, M. H. Hong and S. A. Maier, *Acs Photonics*, 2014, **1**, 1059-1067.
18 R. D. Wang, Q. Wu, Y. Q. Zhang, X. T. Xu, Q. Zhang, W. J. Zhao, B. Zhang, W. Cai, J. H. Yao and J. J. Xu, *Appl. Phys. Lett.*, 2019, **114**, 121102.1-121102.5.
19 A. Tittl, A. Leitis, M. K. Liu, F. Yesilkoy, D. Y. Choi, D. N. Neshev, Y. S. Kivshar and H. Altug, *Science*, 2018, **360**, 1105-1109.
20 M. Gupta, Y. K. Srivastava and R. Singh, *Adv. Mater.*, 2018, **30**,

1704845.1-1704845.8.
21 M. Gupta and R. Singh, *Adv. Opt. Mater.*, 2016, **4**, 2119-2125.
22 X. Chen, W. H. Fan and H. Yan, *Opt. Express*, 2020, **28**, 17102-17112.
23 Y. Meng, F. T. Hu, Y. J. Shen, Y. M. Yang, Q. R. Xiao, X. Fu and M. L. Gong, *Sci. Rep.*, 2018, **8**, 1-11.
24 X. Chen and W. H. Fan, *Opt. Lett.*, 2017, **42**, 2034-2037.
25 X. R. Mao, Y. F. Hang, Y. G. Zhou, J. F. Zhu, Q. Ren, J. M. Zhuo and Y. J. Cai, *IEEE Photonics J.*, 2020, **12**, 1-8.
26 Y. Liu, R. B. Zhong, Z. Lian, C. Bu and S. G. Liu, *Sci. Rep.*, 2018, **8**, 1-8.
27 X. Chen and W. H. Fan, *Nanomaterials*, 2020, **10**, 623.
28 K. I. Bolotin, K. J. Sikes, Z. Jiang, M. Klima, G. Fudenberg, J. Hone, P. Kim and H. L. Stormer, *Solid State Commun.*, 2008, **146**, 351-355.
29 H. Zhu, S. Q. Chen, J. Wen, J. Wang and L. Chen, *Opt. Lett.*, 2019, **44**, 5764-5767.
30 P. Sun and Y. Zou, *Opt. Quant. Electron.*, 2016, **48**.

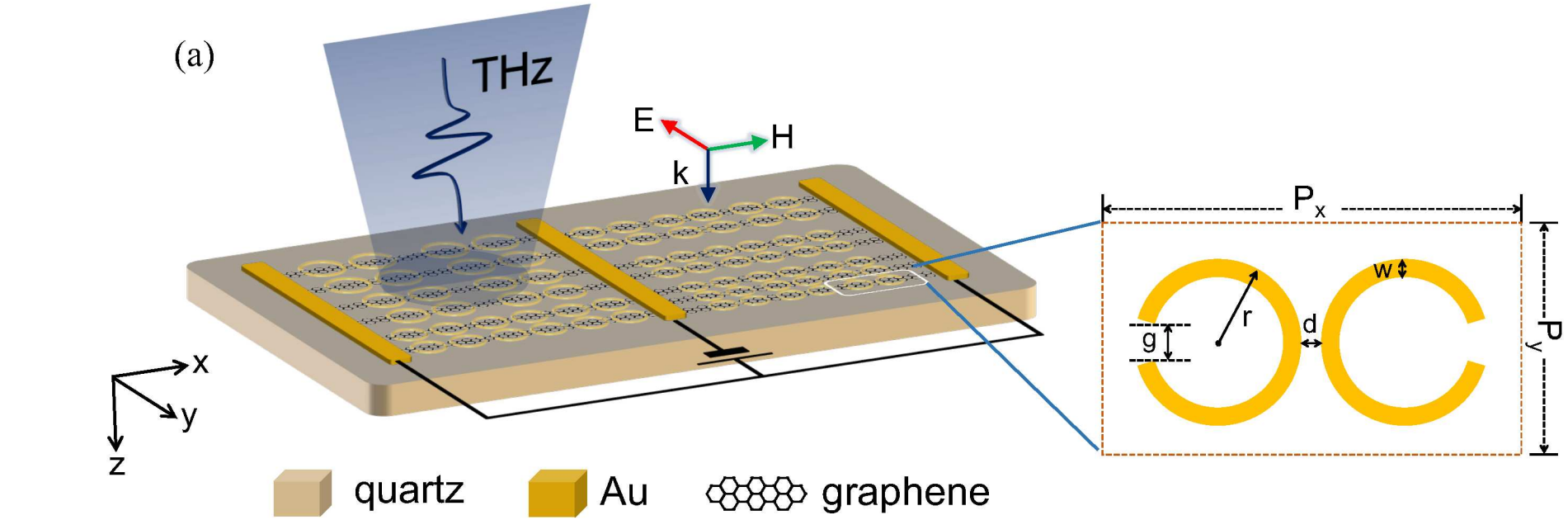
(a)
THz
E
H
k
x
y
z
quartz
Au
graphene
P_x
P_y
w
r
g
d

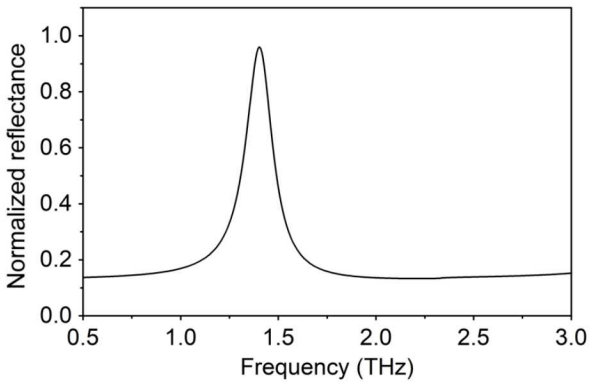
(b)
Normalized reflectance
1.0
0.8
0.6
0.4
0.2
0.0
0.5
1.0
1.5
2.0
2.5
3.0
Frequency (THz)

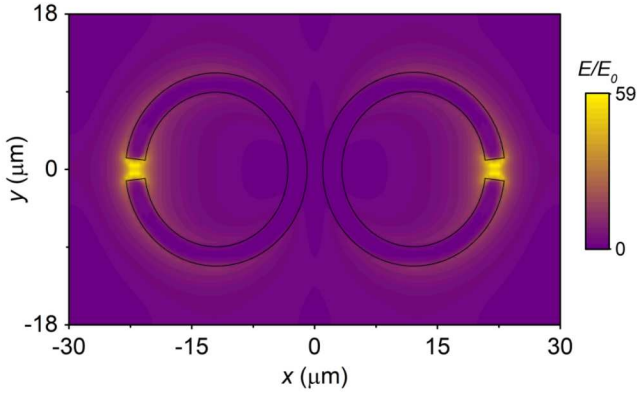
(c)
18
0
-18
y (μm)
-30
-15
0
15
30
x (μm)
E/E_0
59
0

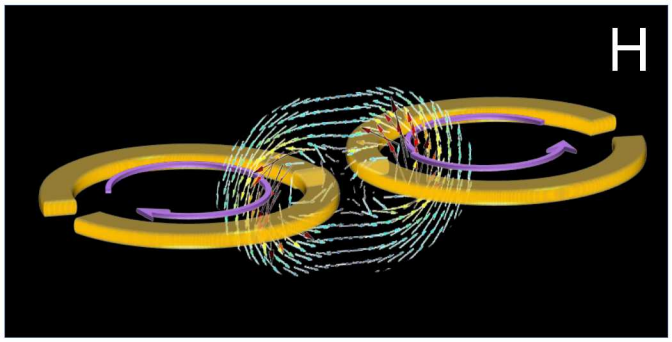
(d)
H

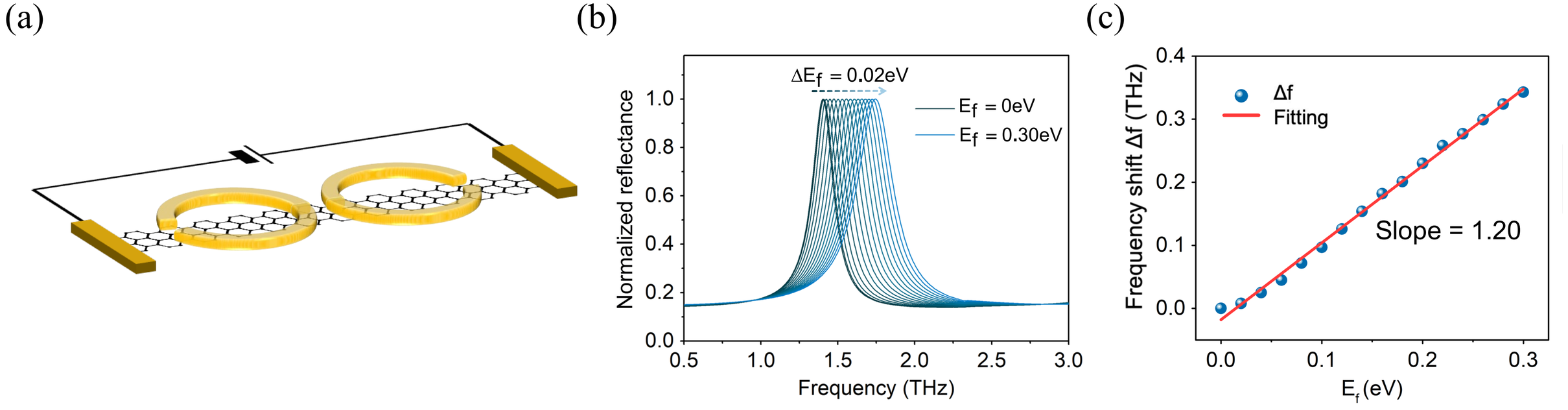
(a)
(b)
ΔEf = 0.02eV
Ef = 0eV
Ef = 0.30eV
Normalized reflectance
Frequency (THz)
(c)
Δf
Fitting
Slope = 1.20
Frequency shift Δf (THz)
Ef (eV)

(a)

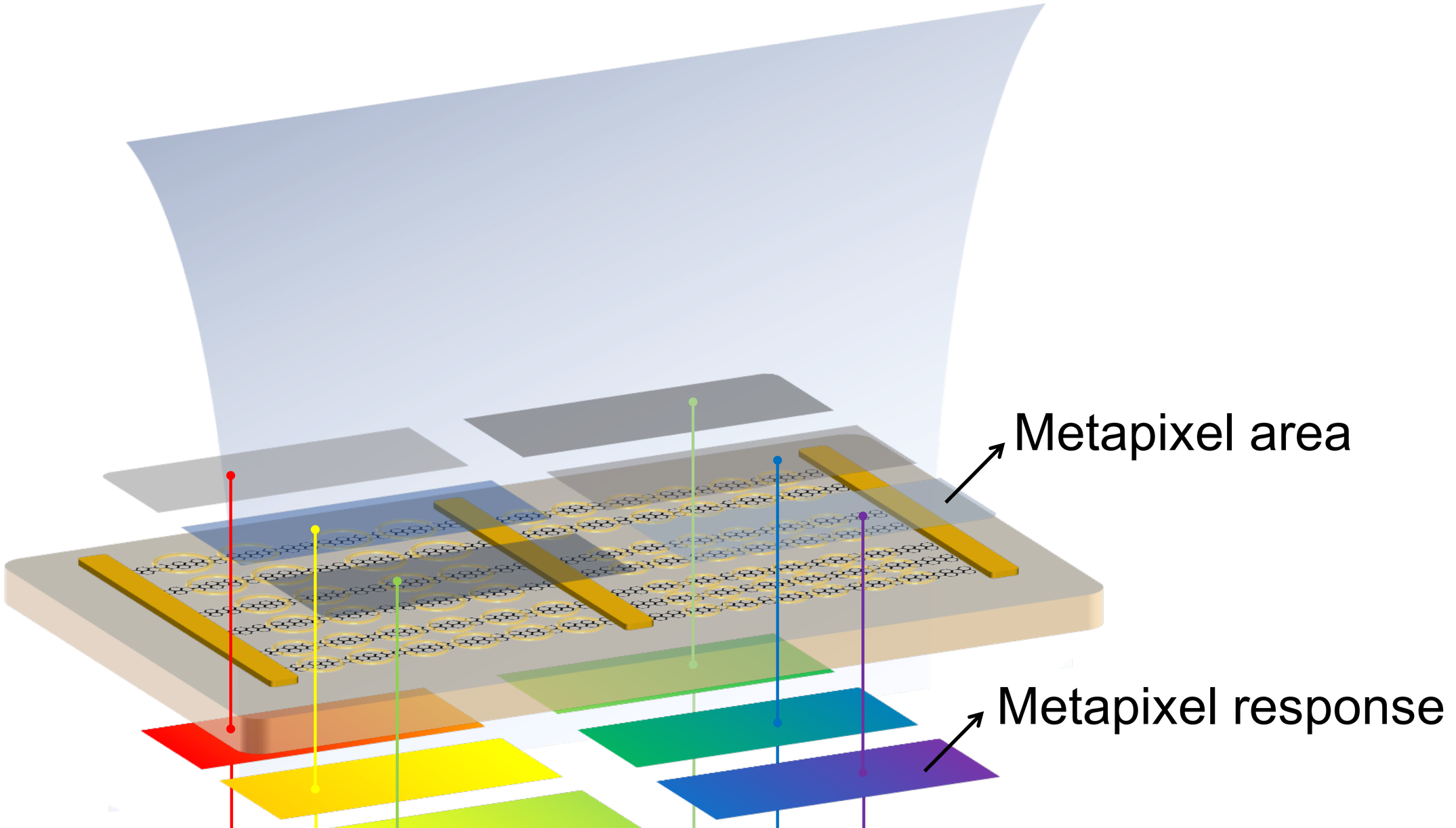
Metapixel area
Metapixel response

(b)

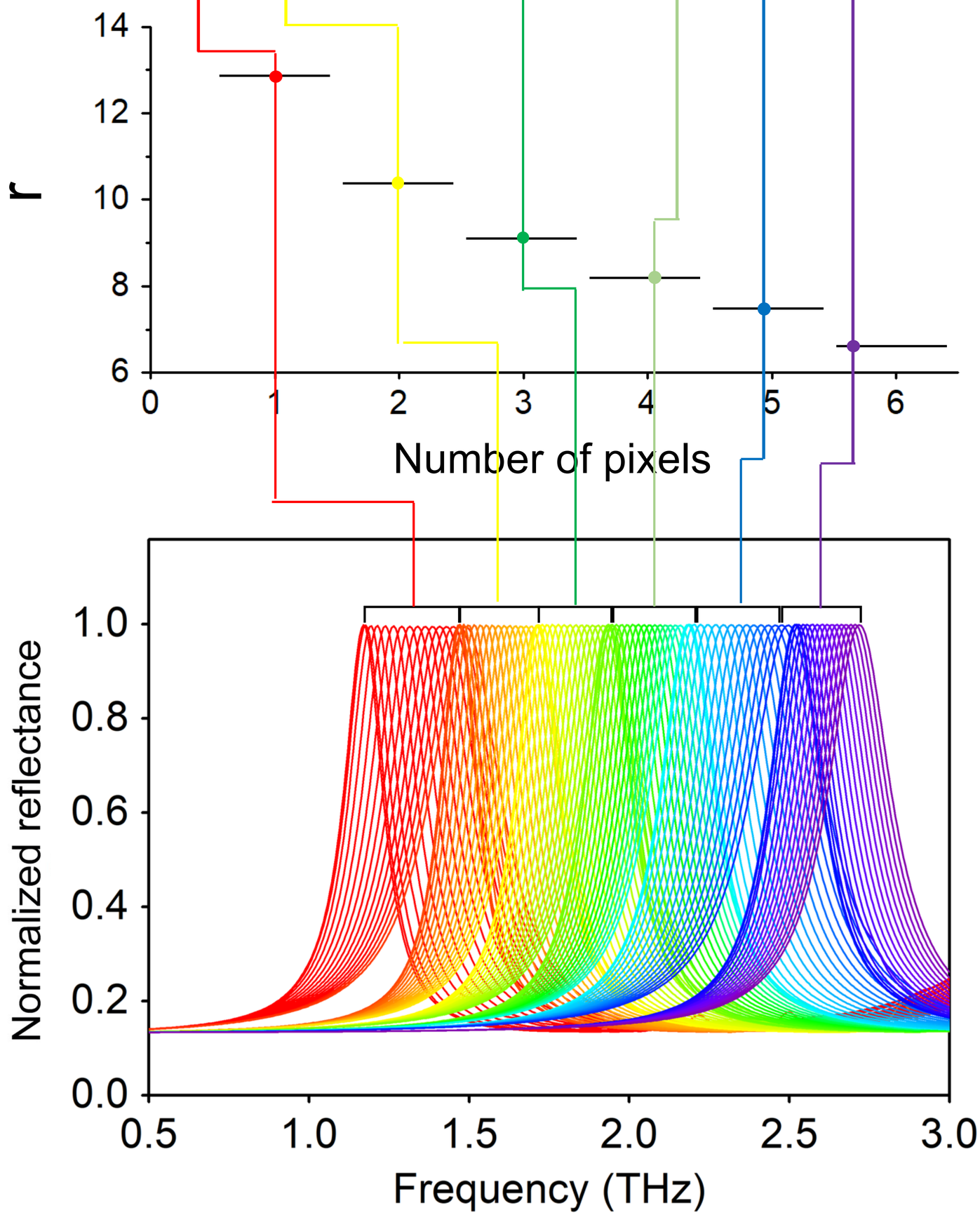
r
14
12
10
8
6
0
1
2
3
4
5
6
Number of pixels

(c)

Normalized reflectance
1.0
0.8
0.6
0.4
0.2
0.0
0.5
1.0
1.5
2.0
2.5
3.0
Frequency (THz)

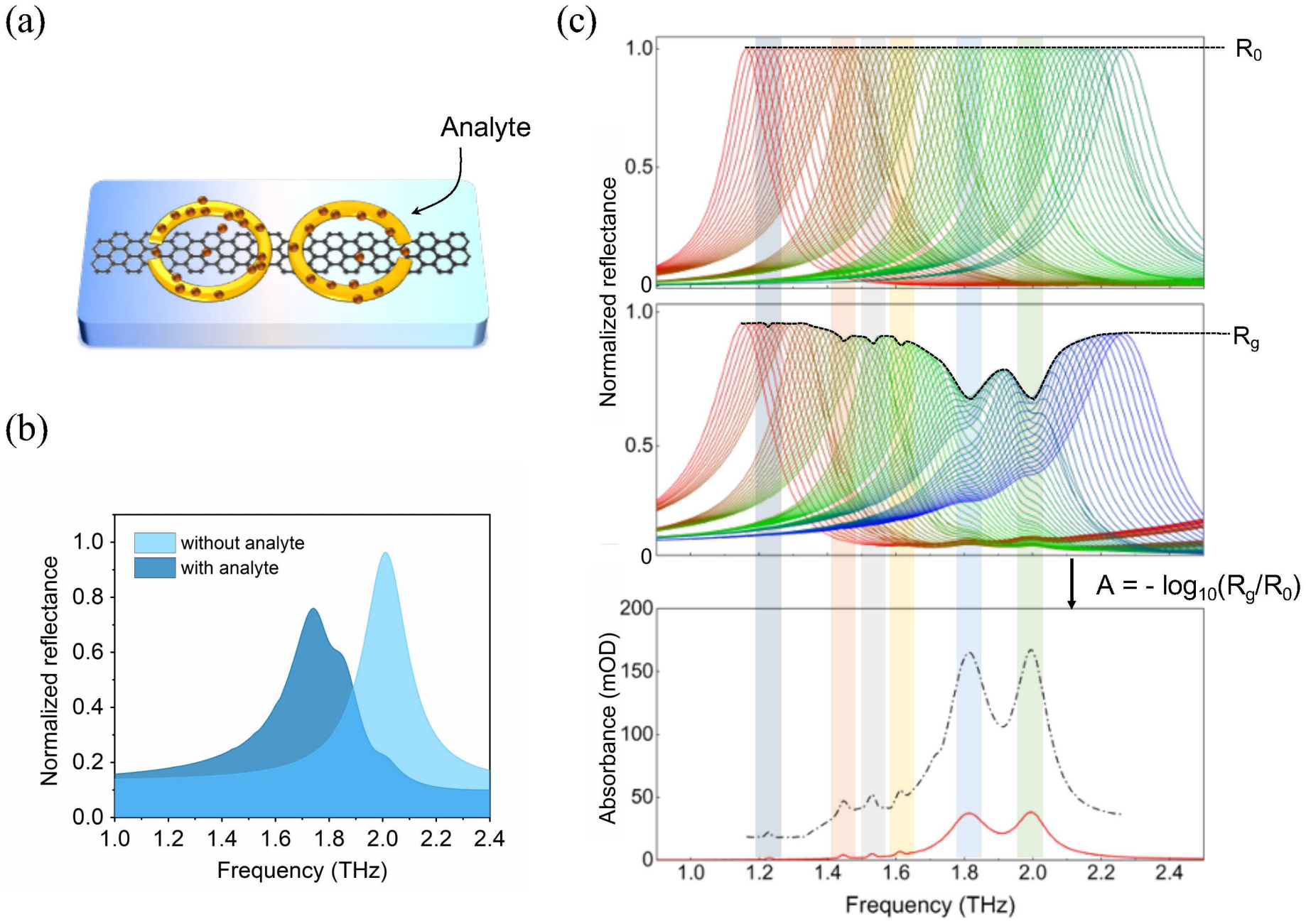
(a)
Analyte
(b)
without analyte
with analyte
Normalized reflectance
Frequency (THz)
(c)
R_0
R_g
Normalized reflectance
$A = - \log_{10}(R_g/R_0)$
Absorbance (mOD)
Frequency (THz)